THE JOURNAL OF PHYSICAL CHEMISTRY A

Article

Cite This: J. Phys. Chem. A 2019, 123, 1894−1903

pubs.acs.org/JPCA

Modeling and Assessment of Afterglow Decay Curves from Thermally Stimulated Luminescence of Complex Garnets

Vasilii M. Khanin,[†,‡] Ivan I. Vrubel,[*,¶] Roman G. Polozkov,[¶] Ivan A. Shelykh,[¶,§] Ivan D. Venevtsev,[∥] Andries Meijerink,[‡] Herfried Wieczorek,[†] Jack Boerekamp,[†] Sandra Spoor,[†] Piotr A. Rodnyi,[∥] and Cees Ronda[†]

[†]Philips Healthcare, High Tech Campus 4, 5656 AE Eindhoven, The Netherlands

[‡]Utrecht University, Princetonplein 5, 3584 CC Utrecht, The Netherlands

[¶]ITMO University, Kronverksky 49, 197101 St. Petersburg, Russia

[§]Science Institute, University of Iceland, Dunhagi 3, IS-107, Reykjavik, Iceland

[∥]Peter the Great St. Petersburg Polytechnic University, Polytekhnicheskaya 29, 195251 St. Petersburg, Russia

Supporting Information

ABSTRACT: Afterglow is an important phenomenon in luminescent materials and can be desired (e.g., persistent phosphors) or undesired (e.g., scintillators). Understanding and predicting afterglow is often based on analysis of thermally stimulated luminescence (TSL) glow curves, assuming the presence of one or more discrete trap states. Here we present a new approach for the description of the time-dependent afterglow from TSL glow curves using a model with a distribution of trap depths. The method is based on the deconvolution of the energy dependent density of occupied traps derived from TSL glow curves using Tikhonov regularization. To test the validity of this new approach, the procedure is applied to experimental TSL and afterglow data for $Lu_1Gd_2Ga_3Al_2O_{12}$:Ce ceramics codoped with 40 ppm of Yb^{3+} or Eu^{3+} traps. The experimentally measured afterglow curves are compared with simulations based on models with and without the continuous trap depth distribution. The analysis clearly demonstrates the presence of a distribution of trap depths and shows that the new approach gives a more accurate description of the experimentally observed afterglow. The new method will be especially useful in understanding and reducing undesired afterglow in scintillators.

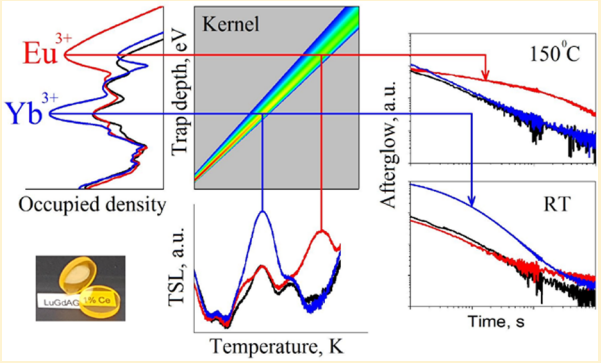

INTRODUCTION

Point defects are mainly responsible for significant delay of light emission in luminescent materials due to temporary charge carrier trapping. This effect finds practical applications, e.g., for the production of emergency signs and luminous paints using persistent phosphors.[1] In other cases, e.g., medical imaging systems and radiation protection, the delayed scintillation response to ionizing radiation is undesired.[2] The understanding of the mechanisms underlying the appearance of slow tails of luminescence (also called afterglow[3]) thus represents an important practical problem.

The influence of the traps on charge carrier transport toward the luminescence centers is generally investigated with thermally stimulated luminescence (TSL) methods or measurements of isothermal decay for the afterglow. The evaluation of the thermal release of carriers from traps with TSL or afterglow methods aims at determination of three trap parameters: the thermal trap depth (E_t), the frequency factor (s) and the kinetic order (b). The most used approaches for processing of the TSL data are first[4] or second[5] kinetic order one trap one recombination center (OTOR) models and interactive kinetics[6] model for traps with discrete energy levels.

Luminescent materials can have more than one type of point defects, which leads to complex TSL peak structures or multicomponent afterglow decay and makes evaluation of experimental data challenging. Several measurement techniques such as varying heating rate method[7] and fractional-heating method[8] have been developed in order to separate contributions from different traps. While these methods procure reliable trap parameters, their implementation is a time-consuming process requiring strict temperature control. The complex glow curve structures have been also considered from the deconvolution point of view.[9]

In research on amorphous materials and glasses an approach of continuous distribution of the energy levels of defects over the band gap is routinely used.[10,11] Rise and decay of the

Received: December 6, 2018
Revised: February 15, 2019
Published: February 18, 2019

DOI: 10.1021/acs.jpca.8b11778
J. Phys. Chem. A 2019, 123, 1894−1903

photocurrent in amorphous semiconductors have been explained by subsequent trapping and release of the carriers from the traps with a continuous distribution of the energy depths.[12]

The same approach has shown a wide trap energy level distribution in evaporated CsI:Tl layers.[13] The model of continuous trap distribution has also been used for wide band gap phosphors, e.g. in.[14,15] Simulation of the afterglow curves shape[16] with the trap level energy distribution has offered an explanation for very slow decay, following a t^{-p} law, with $0 < p < 1$. It should be noted, however, that these trap distribution models are very sensitive to the concentration of the traps and capture and release probabilities for trapping and recombination centers,[16] which are extremely difficult to obtain from afterglow measurements.

TSL is much better suited to access the distribution and properties of the localized states. The evidence of trap depth distribution in luminescent materials is provided by experimentally detected shift of a TSL peak maximum with variations in the preheating temperature T_{stop}.[4,10,17,18]

Garnet crystals of $(Lu,Y)_3Al_5O_{12}$:Cr reveal the distribution of luminescent centers levels in the range 30−50 meV[19] due to the variations in Y/Lu-ions distribution around Cr^{3+} ions. Moreover, nonmonotonous broadening of the fwhm of the trap distribution between 50 to 150 meV has been observed for $Y_3(Al,Ga)_5O_{12}$:Ce,Cr with varying compositions.[20]

In this paper we describe a new method to analyze time-dependent afterglow of garnet scintillators using their TSL glow curves and the trap depth distribution model. The mathematical procedure requires a precalculated (with use of the classic models) frequency factor (s) and consists of two stages. The first step is the deconvolution of the function of the occupied trap density from the experimental TSL signal. The second step is the modeling of the time-dependent afterglow signal at given temperature using the reconstructed occupied trap density function via classical afterglow decay models.

The objects under study are mixed garnet $Lu_1Gd_2Ga_3Al_2O_{12}$:Ce ceramics. The samples have been left nominally pure or codoped with 40 ppm of Yb^{3+} or Eu^{3+} ions, known[21] to be efficient electron traps.[22] Using TSL and afterglow experimental measurements and corresponding numerical modeling, we unambiguously demonstrate the evidence for the distribution of thermal trap depth in the studied samples.

The article is organized into the following sections. At first, we describe experimental evidence of correlation between TSL and afterglow curves and provide evidence for the existence of trap depth distribution through thermal cleaning experiments and the dependence of afterglow curve on irradiation conditions and time. Then we present the mathematical approach for analysis of afterglow using classic (discrete trap depth) TSL models and our new method. Finally, we analyze the results by comparing simulated afterglow behavior based on the different models to experimental data and draw conclusions on the applicability of the new approach.

EXPERIMENTAL SECTION

All $Lu_1Gd_2Ga_3Al_2O_{12}$:Ce 0.2 mol % garnet ceramic samples used in this work, nominally pure or codoped with 40 ppm of Yb^{3+} or Eu^{3+} ions, were prepared in the Philips Research Eindhoven facility by sintering of a mix of base oxides of 4 N purity in air in the form of pills of 14 mm diameter and 2 mm thickness. Cr, Yb, and Eu ions are present as impurities in amounts of less than 1 ppm for starting oxides (supplier information). On the basis of X-ray diffraction patterns, it was concluded that all samples consist of a single garnet phase.

The TSL curves were obtained in the 80−550 K temperature range after irradiation with X-rays (55 kV and 10 mA X-ray tube with molybdenum anode), detected with PMT R6357 in the range of 200−900 nm. The irradiation took place during 5 min; the samples were positioned 3 cm away from the tube. The waiting time between irradiation of the samples and start of the measurements was 10 min; all of the TSL curves shown in the present work were recorded with β = 15 K/min heating rate.

Afterglow curves were measured in the 300−450 K temperature range after 1−6 s of irradiation with X-rays (120 kV, 20−120 mA, 20 cm distance and tungsten anode) detected with a Hamamatsu silicon photodiode and a pico-ammeter Keithley M6485. The estimated absorbed dose was around 20 mGy/s. The curves were recorded in 10−3000 ms and 1−10000 s time ranges and were normalized to the X-ray luminescence intensity of the ceramics at the end of the irradiation pulse.

EXPERIMENTAL RESULTS

Connection between TSL and Afterglow. In this section, we provide the experimental TSL and afterglow curves for the set of $Lu_1Gd_2Ga_3Al_2O_{12}$:Ce ceramics, either doped with Eu^{3+} or Yb^{3+} ions or left nominally pure. We determine the contribution of Yb- and Eu-related traps to the glow curves and correlate both experimental methods with each other.

In the Figure 1 TSL glow curves of the $Lu_1Gd_2Ga_3Al_2O_{12}$:Ce ceramics, nominally pure (reference, curve 1) and doped with

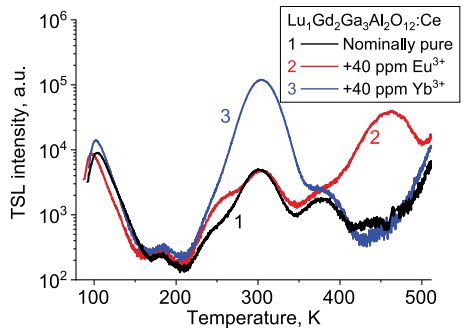

Figure 1. TSL glow curves for $Lu_1Gd_2Ga_3Al_2O_{12}$:Ce ceramics, nominally pure (1) and doped with Eu^{3+} (2) or Yb^{3+} (3).

Eu^{3+} (curve 2) or Yb^{3+} (curve 3) are presented. The samples are characterized by a complex glow curve structure: a TSL peak around 100 K, attributed to antisite defects[23] and a series of TSL peaks in the room temperature region. The latter peaks are related to various residual impurities such as transition metal ions Cr^{3+},[24,25] Ti,[26] V[26] and rare earth (RE)-ions Yb^{3+}[27] and Eu^{3+}.[21] Doping of $Lu_1Gd_2Ga_3Al_2O_{12}$:Ce ceramics with 40 ppm of Yb^{3+} leads to a significant increase of the TSL peak at 305 K (curve 3), while doping with 40 ppm of Eu^{3+} leads to an appearance of an intense peak at 462 K (curve 2).

Previous experiments (partially published in refs 25 and 28) have shown that selection of raw materials sources and codoping with rare-earth ions or 3d transition metals has a strong correlation to experimentally observed TSL peaks. The integral TSL peak intensity is increase with impurity

DOI: 10.1021/acs.jpca.8b11778
J. Phys. Chem. A 2019, 123, 1894−1903

(codopant) content, and any aforementioned impurity-related TSL peak corresponds only to the presence of a specific impurity.

The exact microscopic mechanism of electron capture by impurity-related traps in garnets is still a matter of debate in the community. For phosphates it has been shown indirectly by TSL measurements for $RE^{3+/2+}$ ions[29] and directly by correlation of EPR and TSL for $Eu^{3+/2+}$ [30] that impurity ions themselves are responsible for storage of electrons and creation of specific TSL peaks. On the other hand, using EPR spectra, defect complexes of O^- or oxygen vacancies were shown to be responsible for TSL in perovskites.[31]

In ref 20, it was concluded that in YAGG:Ce,Cr, $Cr^{3+/2+}$ ions on octahedral sites are responsible for storage of electrons and creation of specific TSL peaks, whereas in[32] oxygen vacancies were proposed to act as charge carrier trapping centers. Recently, it has been experimentally shown with transmission spectroscopy that in YAGG:Ce,Yb Yb^{3+} acts as trap by capturing an electron on its 4f shell.[22] In this work, we simply refer to TSL peaks associated with impurities as "Eu- or Yb-related peaks".

Figure 2 displays afterglow curves in the range of 10 ms to 2 h for the studied samples at two temperatures. The curves are

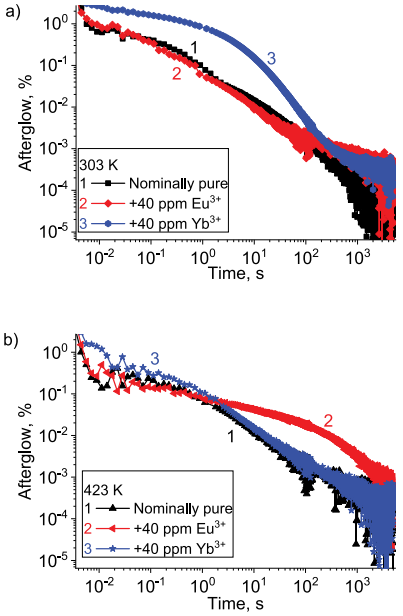

Figure 2. Afterglow curves for $Lu_1Gd_2Ga_3Al_2O_{12}$:Ce ceramics, nominally pure (1) and doped with Eu^{3+} (2) or Yb^{3+} (3): (a) measured at room temperature (303 K) and (b) measured at 423 K.

normalized to 100% at $t = 0$, under steady X-ray excitation. In the Figure 2a one can see that the reference and Eu-codoped samples (curves 1 and 2) have very similar afterglow curve shape at room temperature, while Yb-*co*-doped ceramics has significant additional afterglow component in the time range of 10^{-2}–10^2 s (curve 3). The energy levels of the traps related to Eu^{3+} ions are located deeply in the band gap and they do not contribute to the afterglow of $Lu_1Gd_2Ga_3Al_2O_{12}$:Ce garnets at room temperature. However, at much higher temperature of 423 K (curve 2b), the afterglow curve for Eu-codoped garnet ceramics has an additional component at 10^0–10^4 s (curve 2), while the afterglow of the Yb-co-doped sample resembles the reference curve (curves 1 and 3).

Comparison of the afterglow and TSL curves shows clear correlation between the two experiments. With course of time or with rise of the temperature the electrons released from the traps migrate to the recombination centers (Ce ions with captured holes) and generate emission. The characteristic detrapping time (also called lifetime of carriers on traps[3]) depends on the trap parameters, such as energy depth and frequency factor. In our case, Eu-related traps are observed in the TSL curve (Figure 1) at much higher temperature, compared to the Yb-related ones, and thus have larger trap depth and higher detrapping time, exactly as we observe in the afterglow measurements presented in the Figure 2.

Signs of Trap Depth Distribution. The direct evidence for the existence of a trap depth distribution for $Lu_1Gd_2Ga_3Al_2O_{12}$:Ce,Yb ceramics is obtained from the evolution of TSL glow curves shape with preheating procedure in Figure 3. It was obtained with a special procedure: the

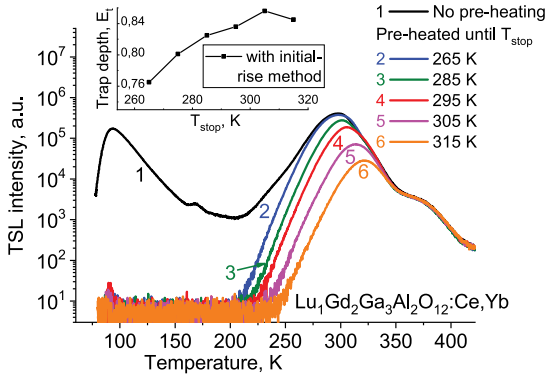

Figure 3. TSL glow curves for $Lu_1Gd_2Ga_3Al_2O_{12}$:Ce ceramics, doped with Yb^{3+}, measured after irradiation with X-rays at 77 K, with no preheating (1) and with preheating to T_{stop} temperature 265 (2), 285 (3), 295 (4), 305 (5), and 315 K (6).

sample had been repeatedly irradiated with the same dose, preheated up to a T_{stop} of 265–315 K, then cooled down and the TSL curve has been measured. The comparison between the obtained curves shows that the TSL peak related to Yb-impurity undergoes a strong shift of the temperature corresponding to the peak maximum (T_m) to higher values with increase of the temperature T_{stop}. Continuous distribution of trap depths E_t can explain the monotonic shift of the TSL peak maximum as a function of subsequent preheating treatments, resulting in the depletion of progressively deeper traps.

With initial-rise method[5] we check the changes in the trap depths with increased T_{stop} temperature, see inset in Figure 3. The smooth variation in the trap depth is an indication of existent trap distribution in our materials.[18]

The signs of the trap depth distribution can be also seen in afterglow measurements. For instance, very slow components corresponding to the range of 10^{-1}–10^2 s and following $t^{-1/2}$ or slower power law decay are clearly visible in the curve 2 of the Figure 2b. Simulation of the time-dependent afterglow[16] showed that the observed behavior is consistent with the trap depth distribution model. Moreover, the superposition of several exponentially decaying components leads to slowing down of the overall afterglow curve until the observed curve resembles the hyperbolic $+t^{-2}$ law[16] (see Figure 2a, curve 3, 10^0–10^2 s time range).

DOI: 10.1021/acs.jpca.8b11778
J. Phys. Chem. A 2019, 123, 1894–1903

Preheating treatment or irradiation at higher temperature with consequent fast cooling down to measurement temperature in the case of the continuous trap density leads to the narrowing of the trap depth distribution and changes in afterglow curve shape. The corresponding results are shown in the Figure 4. The $Lu_1Gd_2Ga_3Al_2O_{12}$:Ce ceramics, doped with

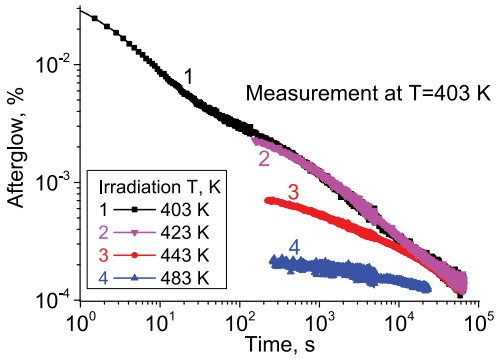

Figure 4. Afterglow curves for $Lu_1Gd_2Ga_3Al_2O_{12}$:Ce ceramics, doped with Eu^{3+}, measured at 403 K after irradiation with X-rays at 403 (1), 423 (2), 443 (3), and 483 K (4) with fast cooling down to measurement temperature afterward.

Eu^{3+}, have been irradiated with X-rays at 403, 423, 443, and 483 K and afterward cooled down to the measurement temperature 403 K. The afterglow curves were not recorded for the period of cooling down process, which took 100−250 s. The resulting curves reveal continuous decrease in afterglow intensity with higher irradiation temperature. The observed variation in the afterglow decay order (from nearly second order ($b = 2$) for curves 1 and 2, Figure 4 to a far slower kinetic order $b = {}^1/_3$ for curve 4, Figure 4), like in case of TSL behavior in Figure 3, is related to the depletion of the shallower part of the trap depth distribution. However, curve 4 in Figure 4 has a limited dynamic range and alternatively can be attributed to influence of deeper traps.

An additional factor that we have to take into account is potential variation in the intensity of the experimentally observed afterglow at the time range comparable to the irradiation duration. Afterglow intensity can be diminished due to a competition between the rate of filling the shallow traps with carriers and fast release of the carriers from them. Figure 5 illustrates this effect: $Lu_1Gd_2Ga_3Al_2O_{12}$:Ce ceramics codoped

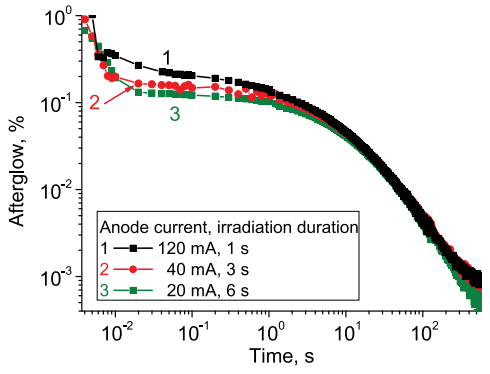

Figure 5. Afterglow curves for $Lu_1Gd_2Ga_3Al_2O_{12}$:Ce ceramics, doped with Yb^{3+}, irradiated with an X-ray tube with conditions of 120 kV, 120 mA for 1 s (1), 120 kV, 40 mA for 3 s (2), and 120 kV, 20 mA for 6 s (3).

with 40 ppm of Yb^{3+} ions has been irradiated several times with a constant dose, but varying dose rates. The X-ray tube was set with a constant anode voltage of 120 kV and varying current from 20 to 120 mA for the duration between 6 and 1 s, keeping absorbed dose constant. One can see that longer irradiation time leads to a decrease in afterglow intensity in the time range of 10^{-2}−10^{0} s.

The dependence of afterglow curve on irradiation conditions can lead to a significant discrepancy between expected results and experimentally observed curves, especially in time windows immediately after X-ray excitation stops, which is highly relevant in the performance of scintillators in, e.g., CT scanners. We develop and implement a simple addition to our models to account for this effect later on in the section "Simulation of the Afterglow Curves"; see Figure 12.

THEORETICAL SECTION

Having determined the contribution of Yb- and Eu-related traps to the glow curves of $Lu_1Gd_2Ga_3Al_2O_{12}$:Ce ceramics and established the evidence for trap depth distribution, we can formulate the models for theoretical simulation of the afterglow.

The band gap diagram of the Figure 6 illustrates the thermoluminescence mechanism we use as the basis for our

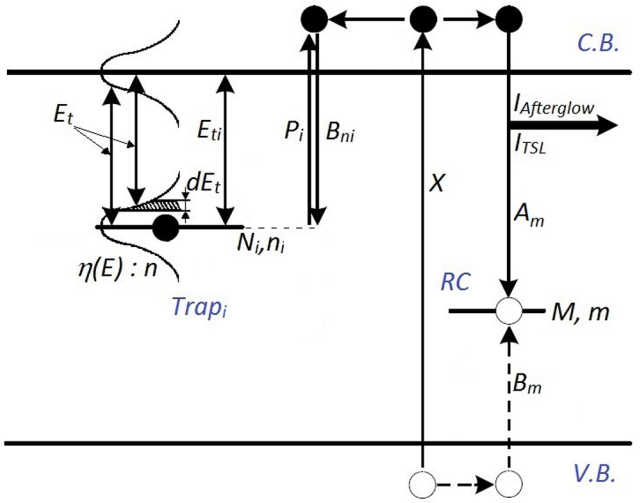

Figure 6. Band diagram, describing the discrete and distributed trap levels located inside the band gap. Free carriers are created by X-ray irradiation with rate X and then become trapped. The holes are trapped on Ce^{3+} ions[40] which thus act as recombination centers for the electrons with corresponding recombination probability coefficient A_m. Electrons are trapped at centers with distributed energy levels. The probability coefficient for the electron capture by the i-trap with energy E_i is denoted as B_{ni} and corresponding release rate as P_i.

simulations. e-h pairs are generated due to absorption of X-ray photons with the rate X, cm^{-3} s^{-1}. Free carriers then become localized at the trapping centers. On the basis of various experimental studies[23,24,33−39] of Ce-doped garnets in our scheme we take into account only electron recombination on Ce^{3+} ions, acting as hole traps.[23,40] The corresponding capture rate for recombination center (RC) can be calculated as product of the concentration of the free electrons n_e, cm^{-3}, the concentration of Ce^{3+} ions having holes captured m, cm^{-3} and recombination probability coefficient A_m, cm·3 s^{-1}.

DOI: 10.1021/acs.jpca.8b11778
J. Phys. Chem. A 2019, 123, 1894−1903

As for electrons, we account for the possibility of their capture by the centers of various origin with different trapping energies E_t, for which we consider both cases of a discrete and continuous distribution. The latter can appear due to the fluctuations of the bottom of the conduction band appearing in mixed solid solutions[41,42] and distortion of the vacuum levels of the defects due to statistical variation of the cations distribution in the second coordination sphere around the defect.[19,43] In the Figure 6 fluctuations of the bottom of the conduction band and energy level of the defects are schematically shown by two bell shaped curves.

Discrete Trap Levels Model. In this model, free electrons created by the irradiation are partially captured by trapping centers with discrete set of the energies E_i. The trapping rate on the center i is calculated as a product of the concentration of the free electrons n_e, cm^{-3}, the concentration of the unoccupied centers of this type N_i, cm^{-3}, and probability coefficient of the electron capture B_{ni}, $cm{\cdot}3\ s^{-1}$.

The escape rate of the electrons from the traps of the type i P_i follows Boltzmann statistics:[3]

$$P_i = s e^{-E_{ti}/kT} \tag{1}$$

where E_{ti} is the thermal depth of the trap counted from the bottom of the conduction band (CB) (thermal ionization energy of the trap), s is the frequency factor, T is the sample temperature, and k is the Boltzmann constant. The frequency factor is usually in the order of the Debye frequency, i.e., is proportional to the number of times per second the trapped charge carrier interacts with phonons.[4]

For simulation of the afterglow generated by discrete number i of traps we need to determine the lifetime of the carriers (or detrapping time) corresponding to the traps of type i (τ_i). The lifetime of carriers τ_i can be either extracted from experimental afterglow curves[28,44] or calculated from trap parameters E_t and s:[3]

$$\tau_i = \frac{1}{P_i} = \frac{1}{s} e^{E_{ti}/kT} \tag{2}$$

Later we implement the $I(t){\cdot}t$-approach[28,45] to extract the values for lifetime of carriers on Yb- and Eu-related traps.

The specific form of the TSL response is determined by several trap parameters: thermal trap depth, frequency factor and kinetic order. For the traps visible in TSL, we use the connection of trap parameters to experimental TSL glow curves via the following expression for first order kinetics:[14]

$$\frac{\beta E_{ti}}{kT_{max}^2} = s{\cdot}e^{-E_{ti}/kT_{max}} \tag{3}$$

where β is the heating rate, E_{ti} is the discrete thermal trap depth, k is the Boltzmann constant, T_{max} is the TSL maximum, s is the frequency factor.

The shape of the afterglow curve with exponential decay (first order discrete trap depth model) is well described by the equation:

$$I_{discr/exp}(t) = \sum_{i=1}^{J} \frac{C{\cdot}n_i}{\tau_i}{\cdot}e^{-t/\tau_i} \tag{4}$$

while for the hyperbolic decay (second order discrete trap depth model) it can be described as

$$I_{discr/hyp}(t) = \sum_{i=1}^{J} C{\cdot}n_i{\cdot}\frac{\tau_i}{(t+\tau_i)^2} \tag{5}$$

where $I_{discr/exp}(t)$ is the simulated afterglow curve using discrete trap levels model with exponential decay, $I_{discr/hyp}(t)$ is the simulated afterglow curve using discrete trap levels model with hyperbolic decay, J is a number of types of traps identified by TSL, n_i is the integral intensity of the TSL peak, related to the i-trap, C is the normalization coefficient, and τ_i is the detrapping time on i-trap.

Trap Depth Distribution Model. In order to simulate the afterglow generated by the continuous distribution of traps we first need to define a way to evaluate the continuous occupied trap density $\eta(E_t)$ from the experimental TSL glow curve. The latter is described by the following integral equation:[4,46]

$$I_{TSL}(T) = \int_{\Delta E} \eta(E_t)\,\ker(T, E_t)\,dE_t \tag{6}$$

where E_t is the thermal trap depth, ΔE is the integration range covering thermal depths of the considered traps, $\eta(E_t)$ is occupied trap density (the function we want to find), and $\ker(E_t, T)$ is the response or kernel function. We have selected the kernel function $\ker(E_t, T)$ following first order kinetics:[14]

$$\ker(T, E_t) = s{\cdot}e^{-E_t/kT}{\cdot}e^{-s/\beta\int_{T_0}^{T} e^{-E_t/kT'}dT'} \tag{7}$$

Here T is the current temperature during linear heating with rate β, s is the frequency factor, and k is the Boltzmann constant. This formula is defined only by intrinsic trap parameters (s and E_t) and does not contain other parameters, namely the total number of traps and their occupations at the beginning of the experiment.

We assume the retrapping probability at the same dE_t interval to be negligible (which is plausible when the selected sampling interval dE_t is small enough) which allows us to use exponential approximation for the kernel function (7). Any number of captures of the electron, which escaped dE_{ti} trap interval, by any other dE_{tj} interval is included in the occupied trap density as the effective shift of the trap depth[5,7] (in the same manner as TSL glow peak is distorted to a more symmetrical shape with a higher T_{max} temperature[47]). A 3D-plot of a kernel function for the first order kinetics TSL glow curve is presented in the Figure 7.

Equation 6 is the Fredholm integral equation of the first kind. Its direct solution presents certain difficulties, because the problem falls into the class of so-called ill-posed problems with respect to the processing of the experimental data.[48,49] We have used the regularization approach proposed by Tikhonov[50] (see the Supporting Information for the details).

When trap depth distribution is found, the afterglow curves can be simulated[4,46] as

$$I_{distr}(t) = C{\cdot}\int_{\Delta E} \eta(E_t){\cdot}\frac{1}{\tau(E_t)} e^{-t/\tau(E_t)}\,dE_t \tag{8}$$

where $\eta(E_t)$ is the trap occupation distribution (Figure 9), C is the normalization coefficient, $\tau(E_t)$ is trap depth dependent lifetime, calculated by using eq 2 for the specific temperature of the measurement for every dE_t sampling interval.

It would also be interesting to develop the distribution model for second order kinetics with corresponding modifications to kernel function. The main challenge is that second order kernel becomes at least a 3-dimensional function of frequency factor (s), thermal trap depth (E_t) and initial

DOI: 10.1021/acs.jpca.8b11778
J. Phys. Chem. A 2019, 123, 1894−1903

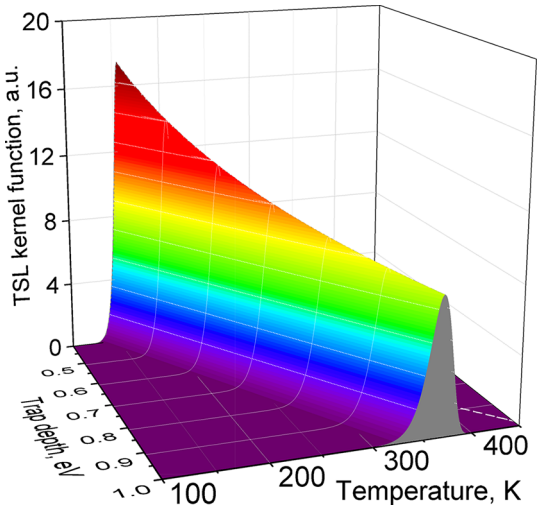

Figure 7. Modeled 3D-plot of the kernel function for the first order kinetics TSL glow curve corresponding to the frequency factor $s = 10^{12}$ s^{-1}.

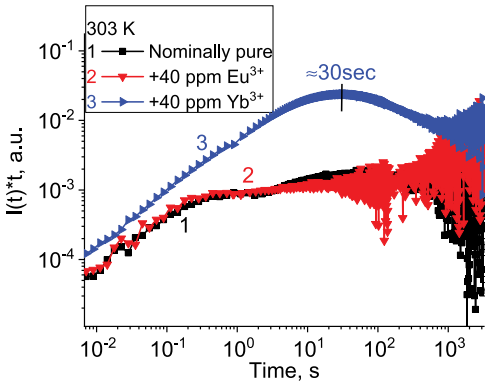

Figure 8. Time-dependent $[I(t)\cdot t]$ functions, constructed from the afterglow curves of Figure 2a for $Lu_1Gd_2Ga_3Al_2O_{12}$:Ce ceramics, nominally pure (1) and doped with Eu^{3+} (2) or Yb^{3+} (3). The maximum of the curve corresponds to the lifetime of carriers on the traps.

population of filled traps (n_0), in which the initial population (n_0) depends on the irradiation dose and X-ray photons penetration depth.

Solving a rate equations system for charge carrier trapping processes and/or additional experiments on saturation of trap filling are required in order to modify the kernel function to accommodate second order kinetics case. It is one of the limitations of the proposed approach, and it is the reason we have conducted experiments (section "Signs of Trap Depth Distribution") to show that trapping/detrapping in our garnet samples follows first order kinetics before using the distribution model. The discrete second order model is used as a contrast.

DISCUSSION

Evaluation of the Glow Curves. Since our modeling requires knowledge of additional parameters, we utilize standard methods to extract them from the TSL[51] and afterglow curves.[44] To estimate the lifetime of the carriers on Yb and Eu-related traps ($\tau_{Yb,Eu}$) the functions $I(t)\cdot t$ have been constructed from afterglow curves of Figure 2a,b. The $I(t)\cdot t$ curves for $Lu_1Gd_2Ga_3Al_2O_{12}$:Ce afterglow measured at room temperature are presented in Figure 8). The observed maximum of the curve (3) corresponds to the lifetime of carriers on Yb-related traps (τ_{Yb}) at room temperature (for detailed explanation of the procedure, please see refs 28 and 45). Corresponding lifetimes of carriers on Yb and Eu-related traps are presented in Table 1.

The trap depth (E_t) and frequency factor (s) are connected with experimental TSL curves by eq 2 and with lifetime of carriers on traps ($\tau_{Yb,Eu}$) by eq 3. We treat eq 2 and eq 3 as an equation system describing the same process with two unknown variables (E_t) and (s). The single solution to the system renders the trap depths $E_t^{Yb} = 0.80 \pm 0.03$ eV and $E_t^{Eu} = 1.22 \pm 0.03$ eV and frequency factor $s = 4 \times 10^{11\pm1}$ s^{-1}. For details of the method, please see ref 28.

Comparable frequency factors, in the range of $s = 10^{11}-10^{13}$ s^{-1}, are reported in the literature for the deep and/or impurity-related traps in complex garnets.[20,52] The data are presented in the Table 1.

We have assigned the constant frequency factor of $s = 4 \times 10^{11}$ s^{-1} to all the impurity related traps in order to simulate afterglow of $Lu_1Gd_2Ga_3Al_2O_{12}$:Ce ceramics in later sections.

Calculation of the Effective Density of the Occupied Traps. The analysis of the properties of the TSL peaks related to Yb and Eu impurities shows that their shape is nearly symmetrical and the so-called geometrical shape factor[7] $\mu = 0.48-0.49$ (kinetic order $b = 1.7$) for both TSL peaks. Symmetrical shape of a TSL peak is attributed to the dominant contribution of retrapping of charge carriers (either by the same kind of traps or by traps of another kind[6]). On the other hand, processing of the afterglow curves for codoped $Lu_1Gd_2Ga_3Al_2O_{12}$:Ce ceramics with May-Partridge method[44] gives the value for the kinetic order $b = 1.5$. This discrepancy can be attributed to the presence of several kinds of traps with similar detrapping time.[3]

Turning to the trap depth distribution model it is worth noting that in the literature, Gaussian[53] or uniform[16] spread of traps depth is normally used. In this work, however, we find suitable distribution shape directly from experimental data using regularization approach without any initial assumptions. The result is presented in the Figure 9. The fwhm of the trap depth distribution is estimated to be 100 meV for both Eu- and Yb-related traps which is in good agreement with existing experimental data.[19,20]

The distribution peaks in the occupied trap density function exhibit nearly Gaussian shape. Probably, this shape of the trap density peaks results from binomial distribution due to the disorder in the nearest Al/Ga (and Lu/Gd) cation distribution of the $Lu_1Gd_2Al_3Ga_2O_{12}$:Ce solid solution. The sensitivity of localized sites to the surrounding cation distribution have been observed with TSL methods in $Y_3(Al,Ga)_5O_{12}$:Ce^{20} and with high-resolution luminescence spectroscopy of (Lu,Tb)$_3Al_5O_{12}$:Cr^{3+}.[19] Additional distortion to the distribution shape may be introduced by weak retrapping from shallow to deeper traps.[47]

One of the restrictions to the model we use is a necessity to use precalculated value for the frequency factor (s). In calculations shown in this section, we have used the same value for $s = 4\cdot 10^{11}$ s^{-1} as in previous section for discrete trap models.

The constant value for frequency factor is an assumption we have to make here in order to simplify the procurement of the trap occupation density. The frequency factor is understood to

DOI: 10.1021/acs.jpca.8b11778
J. Phys. Chem. A 2019, 123, 1894−1903

Table 1. Parameters of Impurity-Related Traps in $Lu_1Gd_2Ga_3Al_2O_{12}$:Ce Ceramics

	experimental lifetime τ_i, s					
Co-dopant	T = 303 K	T = 323 K	T = 423 K	TSL peak T_{max}, K	solving eq 2 and eq 3 as an equation system	trap depth, E_t (eV)
Yb^{3+}	30	7	–	306	→	0.80 ± 0.03
Eu^{3+}	–	–	500	462	$s = 4 \times 10^{11}$ s^{-1}	1.22 ± 0.03

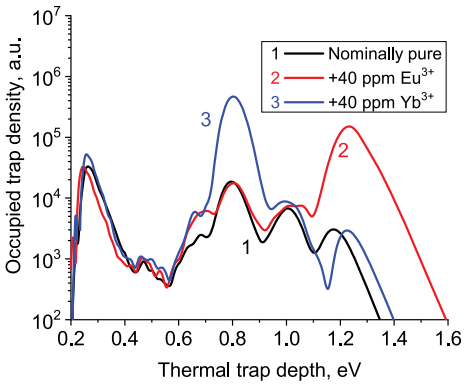

Figure 9. Reconstructed thermal trap depth distribution for nominally pure and codoped with Yb^{3+} and Eu^{3+} $Lu_1Gd_2Ga_3Al_2O_{12}$:Ce samples.

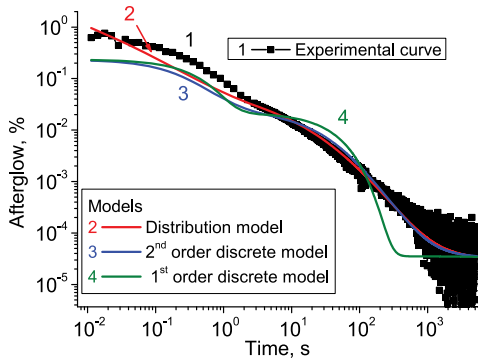

Figure 10. Afterglow curves for nominally pure $Lu_1Gd_2Ga_3Al_2O_{12}$:Ce ceramics at 303 K: measured (1) and modeled with continuous trap depth distribution (2) or discrete trap levels with exponential (3) and hyperbolic decay (4).

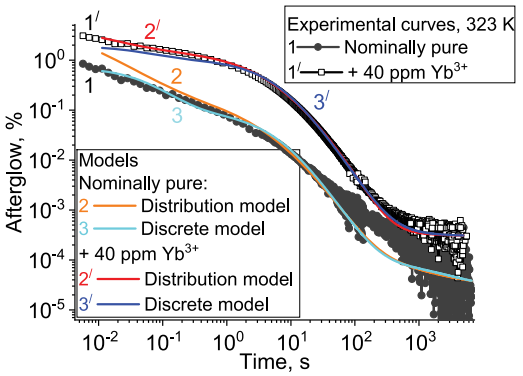

Figure 11. Afterglow curves for $Lu_1Gd_2Ga_3Al_2O_{12}$:Ce ceramics at 323 K: measured for nominally pure sample (1) and codoped with 40 ppm of the Yb^{3+} one (1′) and simulated with continuous trap depth distribution (2, 2′) or discrete trap levels with hyperbolic decay (3, 3′) models.

be dependent on temperature,[3,54] also TSL peaks might have varying underlying luminescence mechanisms (e.g., the case for LYSO:Ce[55]). Instead of the selected frequency factor $s = 4 \times 10^{11}$ s^{-1}, a value lower or higher by an order of magnitude can be used (with corresponding change to E_t), leading to 20% change in the values of calculated detrapping lifetimes. Overall modeled afterglow curve changes its intensity only by a factor of 3 over 9 orders of magnitude change in frequency factor. Details are provided in the Supporting Information.

A further development of the proposed model is allowing that the frequency factor differs from trap-to-trap or even from the left to the right shoulder of the same TSL peak, as the TSL peak in our model is considered to be due to responses from many different traps.

Simulation of the Afterglow Curves. In this section we provide the results of the modeling of afterglow curves using two main approaches: first and second order kinetics discrete trap depth models (in short "discrete models") and trap depth distribution model (in short "distribution model").

We first compare the modeled afterglow curves with the experimental curve for the reference sample of $Lu_1Gd_2Ga_3Al_2O_{12}$:Ce ceramics measured at 303 K (see Figure 10). As absolute values for the trap occupations $\eta(E_t)$ and probability coefficients (B_{ni} and B_m) are unknown the integral area under the simulated afterglow curves is normalized to its experimental value. Comparing experimental afterglow signal and the curves calculated from TSL data one can see that at this temperature the main contribution to the afterglow is given by the Cr- and Yb-related traps.

The first order discrete model is far off the experimental results, while the second order discrete model and distribution model show much better fits. Such a tendency has been obtained for all simulated curves, thus for clarity of the figures we will not show the results of first order kinetics discrete modeling anymore.

To demonstrate further the applicability of our approach we compare the simulated afterglow with experimental data for 323 K, see Figure 11. One can clearly see that the modeled curves fit well to the experimental data for the $Lu_1Gd_2Ga_3Al_2O_{12}$:Ce ceramics, both reference sample and codoped with 40 ppm of Yb^{3+} one over the whole available time range of 10^{-2}–10^4 s. Though with discrete trap model inflection points in the simulated curves are visible, while the inflections are absent in both experimental and distribution model afterglow. On the basis of preheating TSL measurements (Figure 3) and the afterglow simulations, we reason the existence of trap distribution in $Lu_1Gd_2Ga_3Al_2O_{12}$:Ce ceramics.

At much higher temperature of 423 K, the simulation of afterglow curves for $Lu_1Gd_2Ga_3Al_2O_{12}$:Ce ceramics codoped with Eu^{3+} with any model is far off the experimental observations in the ms time range, see dashed curves 2 and 3 Figure 12.

Simulating afterglow from TSL glow curves we need to keep in mind the difference in the irradiation conditions of TSL and afterglow experiments. Low-temperature TSL glow peaks located close to the irradiation temperature are regularly distorted,[56] as they are being partially emptied before the heating-up starts. The same principle holds for the afterglow

DOI: 10.1021/acs.jpca.8b11778
J. Phys. Chem. A 2019, 123, 1894–1903

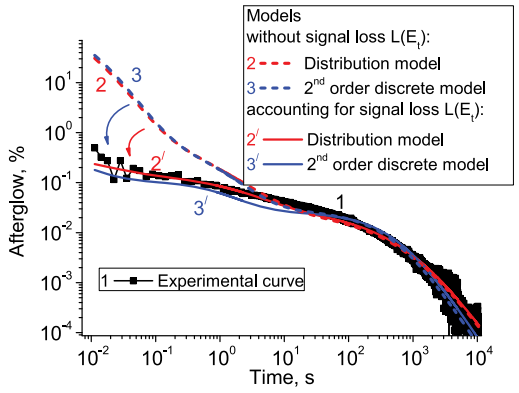

Figure 12. Afterglow curves for $Lu_1Gd_2Ga_3Al_2O_{12}$:Ce ceramics codoped with 40 ppm of Eu^{3+} at 423 K: measured (1) and simulated with continuous trap depth distribution (2) and discrete trap depth model with hyperbolic decay (3) models with (2′, 3′) and without (2, 3) the addition of loss function $L(E_t)$. See eq 10 and eq 11.

measurements. As was shown above in Figure 5, afterglow intensity can be diminished at the time scales shorter or comparable to the duration of the irradiation pulse.[57] The loss function $L(E_t)$ is an estimation of the loss of the trap population due to these artifacts in afterglow experiment:

$$L(E_t) = \frac{\tau(E_t)}{t_{irr_{TSL}}} \times \left(1 - e^{-t_{irr_{AG}}/\tau(E_t)}\right) \quad (9)$$

where $L(E_t)$ is the signal loss for an afterglow experiment, $\tau(E_t)$ = trap depth dependent lifetime, and $t_{irr_{TSL}}$ = duration of the irradiation for TSL measurement.

The derivation of the function is provided in the "Correction of modeled afterglow" section of the Supporting Information. The loss function is especially needed when there is a huge population of shallow traps with lifetimes smaller than (or comparable to) irradiation-pulse duration.

Equation 9 is based on a simple model and does not account for the variation in cross sections of different traps and probability for multiple retrapping on various traps. In order to perform a better estimation for the occupation of shallow traps during irradiation process more complex expression based on nonlinear balance equation[16] has been proposed.

The simulated afterglow curve with trap depth distribution model $I_{distr}^{suppressed}(t)$ adjusted for the signal loss $L(E_t)$ can be computed as

$$I_{distr}^{suppressed}(t) = C \cdot \int_{\Delta E} \eta(E_t) \cdot L(E_t) \cdot \frac{1}{\tau(E_t)} e^{-t/\tau(E_t)}\, dE_t \quad (10)$$

where $\eta(E_t)$ is the trap occupation distribution (Figure 9), C is the normalization coefficient, and $\tau(E_t)$ is the trap depth dependent lifetime, calculated using eq 2 for the specific temperature of the measurement for every dE_t sampling interval.

For the discrete trap levels model adjusted for the signal loss $L(E_t)$ the afterglow curve follows the expression:

$$I_{discr/hyp}^{suppressed}(t) = \sum_{i=1}^{J} C \cdot n_i \cdot L(E_i) \frac{\tau_i}{(t + \tau_i)^2} \quad (11)$$

Here J is the number of identified traps, n_i is the integral intensity of the TSL peak, related to i-trap, C is the normalization coefficient, and τ_i is the carriers' lifetime on the i-trap.

The use of the additional term $L(E_i)$ results in a good fit of the simulated afterglow curves to experimental ones, curve 2′ and 3′ in Figure 12. However, the application of this additional $L(E_i)$ term in eqs 10 and 11 may lead to a worsening of the fit. This is due to the oversimplified model for the signal loss, eq 9.[58,59]

Taking more detailed look at the two models (second order discrete and distributed model), one can notice different results at the inflection points, where the contribution to the afterglow signal from the shallow traps (e.g., Cr) has stopped and the release of the carriers from deeper traps (e.g., Yb) starts playing major role (see curves depicted in Figure 10 at the 10^0–10^1 s time range). Experimental afterglow curve exhibits no discernible inflection points, which demonstrates the role of the continuous trap depth distribution. The latter can be attributed to the various physical reasons: variations in the nearest surrounding of the defect provided by Ga/Al statistical spread over the lattice,[19,43] Anderson localization and fluctuations in the bottom of the conduction band for the electron traps,[41,42] effective broadening of the TSL glow peak due to retrapping processes and polycrystalline nature of the samples.[60]

CONCLUSION

We have developed a new approach for modeling the time-dependent afterglow from TSL glow curves based on a distribution of trap depths instead of discrete trap states as is commonly done. The validity of the approach is tested by simulation of TSL glow curves for $Lu_1Gd_2Ga_3Al_2O_{12}$:Ce ceramics codoped with 40 ppm of Yb^{3+} or Eu^{3+} traps. Comparison of the experimentally observed afterglow with simulated curves based on a continuous distribution or discrete trap depths models reveals that a continuous distribution gives a better description, including the absence of an inflection point which is predicted by discrete trap depth models but not observed experimentally. The trap depth distribution in the new approach is rationalized by disorder in the crystal, which leads to a variation of trap depths for the same type of trap. The better understanding of the cause of the afterglow at different time scales and its relation to TSL glow curves can be used to reduce afterglow in time intervals that are relevant for scintillators in different applications. In general, the role of a distribution of trap depths is important in the analysis of TSL glow curves and afterglow behavior of materials. Including trap depth distributions in TSL and afterglow models can provide more accurate and physically correct modeling of these important phenomena.

ASSOCIATED CONTENT

Supporting Information

The Supporting Information is available free of charge on the ACS Publications website at DOI: 10.1021/acs.jpca.8b11778.

Details on Tikhonov regularization approach, effects of frequency factor variations, and the derivation of the signal loss function eq 9) (PDF

AUTHOR INFORMATION

Corresponding Author

*(I.I.V.) E-mail: ivanvrubel@ya.ru.

ORCID

Ivan I. Vrubel: 0000-0002-8175-0748

Roman G. Polozkov: 0000-0002-6996-3097

DOI: 10.1021/acs.jpca.8b11778
J. Phys. Chem. A 2019, 123, 1894−1903

Andries Meijerink: 0000-0003-3573-9289

Notes

The authors declare no competing financial interest.

■ ACKNOWLEDGMENTS

I.I.V, R.G.P and I.A.S. acknowledge support from the Projects 14.Y26.31.0015 and 3.8884.2017/8.9 of the Ministry of Education and Science of the Russian Federation and Horizon2020 RISE Project CoExAN.

■ REFERENCES

(1) Poelman, D.; Avci, N.; Smet, P. F. Measured Luminance and Visual Appearance of Multi-color Persistent Phosphors. *Opt. Express* **2009**, *17*, 358−364.
(2) van Eijk, C. W. E. Inorganic Scintillators in Medical Imaging. *Phys. Med. Biol.* **2002**, *47*, R85.
(3) McKeever, S. W. S. *Thermoluminescence of Solids*; Cambridge Solid State Science Series; Cambridge University Press: 1985.
(4) Randall, J.; Wilkins, M. Phosphorescence and Electron Traps II. The Interpretation of Long-period 3 Phosphorescence. *Proceedings of the Royal Society of London A: Mathematical, Physical and Engineering Sciences* **1945**, *184*, 390−407.
(5) Klasens, H. A.; Garlick, G.; Gibson, A. Discussion on "The Electron Trap Mechanism of Luminescence in Sulphide and Silicate Phosphors. *Proc. Phys. Soc.* **1948**, *61*, 101.
(6) Sunta, C. M.; Kulkarni, R. N.; Yoshimura, E. M.; Mol, A. W.; Piters, T. M.; Okuno, E. Interactive Kinetics in Thermoluminescence (TL) and Its Effect on Glow Curves and Their Growth as a Function of Dose. *Phys. Status Solidi B* **1994**, *186*, 199−208.
(7) Chen, R.; Winer, S. A. A. Effects of Various Heating Rates on Glow Curves. *J. Appl. Phys.* **1970**, *41*, 5227−5232.
(8) Gobrecht, H.; Hofmann, D. Spectroscopy of Traps by Fractional Glow Technique. *J. Phys. Chem. Solids* **1966**, *27*, 509−522.
(9) Sadek, A.; Eissa, H.; Basha, A.; Kitis, G. Development of the Peak Fitting and Peak Shape Methods to Analyze the Thermoluminescence Glow-curves Generated with Exponential Heating Function. *Nucl. Instrum. Methods Phys. Res., Sect. B* **2014**, *330*, 103−107.
(10) Martini, M.; Spinolo, G.; Vedda, A.; Arena, C. Phosphorescence and Thermally Stimulated Luminescence of Amorphous SiO2. *Solid State Commun.* **1994**, *91*, 751−756.
(11) Nikl, M.; Nitsch, K.; Mihokova, E.; Solovieva, N.; Mares, J. A.; Fabeni, P.; Pazzi, G. P.; Martini, M.; Vedda, A.; Baccaro, S. Efficient Radioluminescence of the Ce3+-doped NaGd Phosphate Glasses. *Appl. Phys. Lett.* **2000**, *77*, 2159−2161.
(12) Wieczorek, H. Measurement and Simulation of the Dynamic Performance of a-Si:H Image Sensors. *J. Non-Cryst. Solids* **1993**, *164*, 781−784.
(13) Wieczorek, H.; Overdick, M. Afterglow and Hysteresis in CsI:Tl. *Proceedings of the 5th International Conference on Inorganic Scintillators and Their Applications (SCINT99) 2000* **2000**, 385−390.
(14) Randall, J.; Wilkins, M. Phosphorescence and Electron Traps - I. The Study of Trap Distributions. *Proceedings of the Royal Society of London A: Mathematical, Physical and Engineering Sciences 1945* **1945**, *184*, 365−389.
(15) Srivastava, J. K.; Supe, S. J. Trap Distribution Analysis for Thermoluminescence of CaSO4:Dy. *J. Phys. D: Appl. Phys.* **1983**, *16*, 1813.
(16) Hornyak, W.; Franklin, A. Single Level Isothermal TL-decay (with Energy Level Distribution and Retrapping). *Nucl. Tracks Radiat. Meas.* **1988**, *14*, 81−89.
(17) Van den Eeckhout, K.; Bos, A. J. J.; Poelman, D.; Smet, P. F. Revealing Trap Depth Distributions in Persistent Phosphors. *Phys. Rev. B: Condens. Matter Mater. Phys.* **2013**, *87*, 045126.
(18) Brylew, K.; Drozdowski, W.; Wojtowicz, A. J.; Kamada, K.; Yoshikawa, A. Studies of Low Temperature Thermoluminescence of GAGG:Ce and LuAG:Pr Scintillator Crystals Using the TmaxTstop Method. *J. Lumin.* **2014**, *154*, 452−457.
(19) Feofilov, S.; Kulinkin, A.; Ovanesyan, K.; Petrosyan, A. Discrete Zero-phonon Cr3+ Lines in the Spectra of TerbiumYttriumLutetium Aluminum Garnets Solid Solutions: Lattice Compression and Dilation. *Solid State Commun.* **2016**, *226*, 39−43.
(20) Ueda, J.; Dorenbos, P.; Bos, A. J. J.; Kuroishi, K.; Tanabe, S. Control of Electron Transfer Between Ce^{3+} and Cr^{3+} in the $Y_3Al_{5-x}Ga_xO_{12}$ Host Via Conduction Band Engineering. *J. Mater. Chem. C* **2015**, *3*, 5642−5651.
(21) Milliken, E.; Oliveira, L.; Denis, G.; Yukihara, E. Testing a Model-guided Approach to the Development of New Thermoluminescent Materials Using YAG:Ln Produced by Solution Combustion Synthesis. *J. Lumin.* **2012**, *132*, 2495−2504.
(22) Ueda, J.; Miyano, S.; Tanabe, S. Formation of Deep Electron Traps by Yb3+ Codoping Leads to Super-long Persistent Luminescence in Ce3+-doped Yttrium Aluminum Gallium Garnet Phosphors. *ACS Appl. Mater. Interfaces* **2018**, *10*, 20652−20660.
(23) Fasoli, M.; Vedda, A.; Nikl, M.; Jiang, C.; Uberuaga, B. P.; Andersson, D. A.; McClellan, K. J.; Stanek, C. R. Band-gap Engineering for Removing Shallow Traps in Rare-earth $Lu_3Al_5O_{12}$ Garnet Scintillators Using Ga^{3+} Doping. *Phys. Rev. B: Condens. Matter Mater. Phys.* **2011**, *84*, 081102.
(24) Ueda, J.; Kuroishi, K.; Tanabe, S. Bright Persistent Ceramic Phosphors of Ce^{3+}-Cr^{3+}-codoped Garnet Able to Store by Blue Light. *Appl. Phys. Lett.* **2014**, *104*, 101904.
(25) Khanin, V.; Venevtsev, I.; Rodnyi, P.; Ronda, C. Changes in Trap Parameters in Various mixed Oxide Garnets. *Radiat. Meas.* **2016**, *90*, 104−108.
(26) Ueda, J.; Hashimoto, A.; Takemura, S.; Ogasawara, K.; Dorenbos, P.; Tanabe, S. Vacuum Referred Binding Energy of 3d Transition Metal Ions for Persistent and Photostimulated Luminescence Phosphors of Cerium-doped Garnets. *J. Lumin.* **2017**, *192*, 371−375.
(27) You, F.; Bos, A. J. J.; Shi, Q.; Huang, S.; Dorenbos, P. Electron Transfer Process Between Ce^{3+} Donor and Yb^{3+} Acceptor Levels in the Bandgap of $Y_3Al_5O_{12}$ (YAG). *J. Phys.: Condens. Matter* **2011**, *23*, 215502.
(28) Khanin, V.; Venevtsev, I.; Spoor, S.; Boerekamp, J.; van Dongen, A.-M.; Wieczorek, H.; Chernenko, K.; Buettner, D.; Ronda, C.; Rodnyi, P. A New Method for Unambiguous Determination of Trap Parameters From Afterglow and TSL Curves Connection: Example on Garnets. *Opt. Mater.* **2017**, *72*, 161−168.
(29) Bos, A. J.; Dorenbos, P.; Bessière, A.; Lecointre, A.; Bedu, M.; Bettinelli, M.; Piccinelli, F. Study of TL Glow Curves of YPO4 Double Doped with Lanthanide Ions. *Radiat. Meas.* **2011**, *46*, 1410−1416.
(30) Zeler, J.; Zych, E. On the Thermoluminescence Properties and Mechanism of LuPO4:Eu Sintered Materials. *RSC Adv.* **2016**, *6*, 89019−89027.
(31) Vedda, A.; Fasoli, M.; Nikl, M.; Laguta, V. V.; Mihokova, E.; Pejchal, J.; Yoshikawa, A.; Zhuravleva, M. Trap-center Recombination Processes by Rare Earth Activators in $YAlO_3$ Single Crystal Host. *Phys. Rev. B: Condens. Matter Mater. Phys.* **2009**, *80*, 045113.
(32) Varney, C.; Selim, F. Positron Lifetime Measurements of Vacancy Defects in Complex Oxides. *Acta Phys. Pol., A* **2014**, *125*, 764−766.
(33) Nikl, M.; Kamada, K.; Babin, V.; Pejchal, J.; Pilarova, K.; Mihokova, E.; Beitlerova, A.; Bartosiewicz, K.; Kurosawa, S.; Yoshikawa, A. Defect Engineering in Ce-doped Aluminum Garnet Single Crystal Scintillators. *Cryst. Growth Des.* **2014**, *14*, 4827−4833.
(34) Nikl, M.; Mihokova, E.; Pejchal, J.; Vedda, A.; Zorenko, Y.; Nejezchleb, K. The Antisite LuAl Defect-related Trap in Lu3Al5O12:Ce Single Crystal. *Phys. Status Solidi B* **2005**, *242*, R119−R121.
(35) Khanin, V. M.; Rodnyi, P. A.; Wieczorek, H.; Ronda, C. R. Electron Traps in Gd3Ga3Al2O12:Ce Garnets Doped with Rare-earth Ions. *Tech. Phys. Lett.* **2017**, *43*, 439−442.
(36) Ueda, J.; Dorenbos, P.; Bos, A. J. J.; Meijerink, A.; Tanabe, S. Insight into the Thermal Quenching Mechanism for Y3Al5O12:Ce3+ Through Thermoluminescence Excitation Spectroscopy. *J. Phys. Chem. C* **2015**, *119*, 25003−25008.

DOI: 10.1021/acs.jpca.8b11778
J. Phys. Chem. A 2019, 123, 1894−1903

(37) Xia, Z.; Meijerink, A. Ce3+-Doped Garnet Phosphors: Composition Modification, Luminescence Properties and Applications. *Chem. Soc. Rev.* **2017**, *46*, 275−299.
(38) Luo, Y.; Xia, Z. Effect of Al/Ga Substitution on Photoluminescence and Phosphorescence Properties of Garnet-Type Y3Sc2Ga3xAlxO12:Ce3+ Phosphor. *J. Phys. Chem. C* **2014**, *118*, 23297−23305.
(39) Wu, H.; Yang, C.; Zhang, Z.; Tang, Y. Photoluminescence and Thermoluminescence of Ce3+ Incorporated Y3Al5O12 Synthesized by Rapid Combustion. *Optik* **2016**, *127*, 1368−1371.
(40) Romanov, N. G.; Tolmachev, D. O.; Gurin, A. S.; Uspenskaya, Y. A.; Asatryan, H. R.; Badalyan, A. G.; Baranov, P. G.; Wieczorek, H.; Ronda, C. Dramatic Impact of the Giant Local Magnetic Fields on Spin-dependent Recombination Processes in Gadolinium Based Garnets. *Appl. Phys. Lett.* **2015**, *106*, 262404.
(41) Gektin, A. V.; Belsky, A. N.; Vasil'ev, A. N. Scintillation Efficiency Improvement by Mixed Crystal Use. *IEEE Trans. Nucl. Sci.* **2014**, *61*, 262−270.
(42) Belsky, A.; Gektin, A.; Gridin, S.; Vasil'ev, A. N. Electronic and Optical Properties of Scintillators Based on Mixed Ionic Crystals. *Springer Proc. Phys.* **2017**, *200*, 63−82.
(43) Laguta, V.; Zorenko, Y.; Gorbenko, V.; Iskaliyeva, A.; Zagorodniy, Y.; Sidletskiy, O.; Bilski, P.; Twardak, A.; Nikl, M. Aluminum and Gallium Substitution in Yttrium and Lutetium AluminumGallium Garnets: Investigation by Single-crystal NMR and TSL Methods. *J. Phys. Chem. C* **2016**, *120*, 24400−24408.
(44) May, C. E.; Partridge, J. A. Thermoluminescent Kinetics of Alphairradiated Alkali Halides. *J. Chem. Phys.* **1964**, *40*, 1401−1409.
(45) Simmons, J. G.; Tam, M. C. Theory of Isothermal Currents and the Direct Determination of Trap Parameters in Semiconductors and Insulators Containing Arbitrary Trap Distributions. *Phys. Rev. B* **1973**, *7*, 3706−3713.
(46) Hornyak, W. F.; Chen, R. Thermoluminescence and Phosphorescence with a Continuous Distribution of Activation Energies. *J. Lumin.* **1989**, *44*, 73−81.
(47) Kelly, P.; Braunlich, P. Phenomenological Theory of Thermoluminescence. *Phys. Rev. B* **1970**, *1*, 1587−1595.
(48) Phillips, D. L. A Technique for the Numerical Solution of Certain Integral Equations of the First Kind. *J. Assoc. Comput. Mach.* **1962**, *9*, 84−97.
(49) Wazwaz, A.-M. The Regularization Method for Fredholm Integral Equations of the First Kind. *Comp. Math. Appl.* **2011**, *61*, 2981−2986.
(50) Tikhonov, A. N.; Arsenin, V. Y. *Solution of Ill-Posed Problems*; Winston & Sons: WA, 1977.
(51) Pagonis, V.; Kitis, G.; Furreta, C. *Numerical and Practical Exercises in Thermoluminescence*; Springer: New York, 2006.
(52) Mihokova, E.; Vavru, K.; Kamada, K.; Babin, V.; Yoshikawa, A.; Nikl, M. Deep Trapping States in Cerium Doped (Lu,Y,Gd)3-(Ga,Al)5O12 Single Crystal Scintillators. *Radiat. Meas.* **2013**, *56*, 98−101 Proceedings of the 8th International Conference on Luminescent Detectors and Transformers of Ionizing Radiation (LUMDETR 2012) .
(53) Medlin, W. L. Decay of Phosphorescence from a Distribution of Trapping Levels. *Phys. Rev.* **1961**, *123*, 502−509.
(54) Chen, R. Glow Curves with General Order Kinetics. *J. Electrochem. Soc.* **1969**, *116*, 1254−1257.
(55) Vedda, A.; Nikl, M.; Fasoli, M.; Mihokova, E.; Pejchal, J.; Dusek, M.; Ren, G.; Stanek, C. R.; McClellan, K. J.; Byler, D. D. Thermally Stimulated Tunneling in Rare-earth-doped Oxyorthosilicates. *Phys. Rev. B: Condens. Matter Mater. Phys.* **2008**, *78*, 195123.
(56) Sunta, C. *Unraveling Thermoluminescence*; Springer: 2015.
(57) Wieczorek, H. Transient Currents in a-Si:H Diodes. *J. Non-Cryst. Solids* **1991**, *137*, 1309−1312.
(58) Kelly, P.; Laubitz, M. J.; Braunlich, P. Exact Solutions of the Kinetic Equations Governing Thermally Stimulated Luminescence and Conductivity. *Phys. Rev. B* **1971**, *4*, 1960−1968.
(59) Sunta, C. M.; Ayta, W. E. F.; Kulkarni, R. N.; Chubaci, J. F. D.; Watanabe, S. The Quasi-equilibrium Approximation and its Validity for the Thermoluminescence of Inorganic Phosphors. *J. Phys. D: Appl. Phys.* **1999**, *32*, 717.
(60) Shen, Y.; Shi, Y.; Feng, X.; Pan, Y.; Li, J.; Zeng, Y.; Nikl, M.; Krasnikov, A.; Vedda, A.; Moretti, F. The Harmful Effects of Sintering Aids in Pr:LuAG Optical Ceramic Scintillator. *J. Am. Ceram. Soc.* **2012**, *95*, 2130−2132.

DOI: 10.1021/acs.jpca.8b11778
J. Phys. Chem. A 2019, 123, 1894−1903